Nano Energy (2013) 2, 951–957

Available online at www.sciencedirect.com

ScienceDirect

journal homepage: www.elsevier.com/locate/nanoenergy

RAPID COMMUNICATION

Rational geometrical design of multi-diameter nanopillars for efficient light harvesting

Bo Hua[a], Baomin Wang[b], Miao Yu[a], Paul W. Leu[b], Zhiyong Fan[a,*]

[a]Department of Electronic and Computer Engineering, Hong Kong University of Science and Technology, Clear Water Bay, Kowloon, Hong Kong SAR, China
[b]Department of Industrial Engineering, University of Pittsburgh, Pittsburgh, PA 15261, USA

Received 19 January 2013; received in revised form 19 March 2013; accepted 19 March 2013
Available online 29 March 2013

KEYWORDS
Nanostructure;
Nanopillar;
Transverse resonance mode;
Multi-diameter;
Nanocone;
Light harvesting

Abstract
Three-dimensional arrays of nanostructures have drawn increasing attention for solar energy harvesting in recent years. In this work, with Ge as the model material, the broadband solar spectrum absorption of arrays of multi-diameter nanopillars is explored with finite difference time domain simulations. It is found that light absorption of a nanopillar array is either determined by the material filling ratio or by transverse resonance leaky modes depending on input wavelength. A properly designed multi-diameter nanopillar array can compete with a nanocone array on broadband light absorption capability. As single crystalline multi-diameter nanopillars can be grown with a bottom-up approach, the investigation here provides important design guidelines for the fabrication of efficient nanostructured photovoltaic and other optoelectronic devices.

Introduction

Three-dimensional (3-D) arrays of nanostructures, including nanowires (NWs) [1–8], nanopillars (NPLs) [9,10], nanocones (NCNs) [11–16], nanowells [17], nanoshells [18], etc., have demonstrated intriguing optical properties such as efficient light trapping for broadband wavelength and large incident angle [11,19]. These properties are not only of fundamental interest to understand light-matter interaction at the nanoscale, but also of technological usefulness for applications such as photovoltaics, photodetection, and light emitting devices, etc. Particularly for optoelectronic applications, research has discovered that 3-D nanostructures can not only lead to improved photon harvesting utilizing light trapping mechanism, but also enhance photo-carrier collection efficiency due to shortened diffusion length [20–22]. On the other hand, it has been shown that the geometrical factors of nanostructure arrays including the shape of the individual structures and the pitch/periodicity play an important role in determining their optical properties [1,3–7,10,14,19,20]. Therefore, rational structural design has to be applied in order to fabricate an efficient optoelectronic device. In the past we have demonstrated fabrication of shape engineered

*Corresponding author. Tel.: +852 2358 8027; fax: +852 2358 1485.
E-mail address: eezfan@ust.hk (Z. Fan).

2211-2855/$ - see front matter © 2013 Elsevier Ltd. All rights reserved.
http://dx.doi.org/10.1016/j.nanoen.2013.03.016

NPLs showing improved light absorption capability in comparison to single diameter NPLs (SNPLs) [10]. In this work, a more systematic investigation is carried out in order to further understand light coupling, propagation and absorption in NPL arrays. It is found that for short wavelength light, the absorption capability of the structure largely depends on the array material filling ratio, whereas for long wavelength light, waveguide modes determine light coupling and absorption efficiency in NPLs. More importantly, shape design of NPLs is explored and optical properties of multi-diameter NPLs (MNPLs) including dual-diameter NPLs (DNPLs) are investigated. It is discovered that absorption of MNPLs approaches that of NCNs when the number of the segments ***N*** increases, with ***N***=7 yielding the same light absorption level to NCNs. As the single crystalline MNPLs can be grown with catalytic vapor transport [10], the investigation here can shed light on optimal design of high quality light harvesting NPLs with bottom-up approach.

Simulation method

The schematic of the hexagonal Ge SNPL, DNPL, MNPL and NCN arrays is shown in Figure 1. The lengths/heights of the NPL arrays and the NCN arrays are all 2000 nm, which follows our previous work [23]. The optical properties are calculated by finite difference time domain method (Lumerical FDTD Solutions 8.5). In our simulations, the mesh size is set as 6 points per wavelength (PPW) when calculating the reflection and transmission, namely $\lambda/6\boldsymbol{n}$, where ***n*** represents material refractive index. When calculating the E field distribution and optical absorption profiles, the mesh size is set as 2 nm in order to obtain high resolution plot. For the top and the bottom surface, perfectly matched layer (PML) boundary conditions are used. According to the conservation of energy, the absorption is calculated as $A(\lambda) = 1 - R(\lambda) - T(\lambda)$, where the range of incident source wavelength λ is set as 300–2000 nm, considering the band gap of Ge and the solar spectrum. After the absorption curve is obtained, the broadband-integrated absorption is calculated by the following equation:

$$A = \frac{\int_{\lambda_{min}}^{\lambda_{max}} (I(\lambda)A(\lambda)\lambda/hc)d\lambda}{\int_{\lambda_{min}}^{\lambda_{max}} (I(\lambda)\lambda/hc)d\lambda} \quad (1)$$

where λ_{max} is 2000 nm, λ_{min} is 300 nm, ***h*** is the Plank constant, ***c*** is the speed of light in free space, and $I(\lambda)$ is the spectral irradiance of the Air Mass 1.5 Global spectrum. The broadband-integrated absorption values as a function of different NPL pitches and diameters are plotted by Matlab (Version 7.14.0.739) as a 2-dimentional (2-D) contour after interpolation, with a pitch range ***p*** of 50 to 2000 nm and diameter $\boldsymbol{d} \leq \boldsymbol{p}$. The broadband-integrated transmittance and broadband-integrated reflectance 2-D contours are also calculated and plotted in the same way.

Result and discussion

Figure 2a shows the broadband-integrated reflectance of the SNPL arrays as a function of pitch (x-axis) and diameter (y-axis). It can be seen that the reflectance simply depends on the material filling ratio $FR = \pi d^2/2\sqrt{3}a^2$, where ***a*** is the pitch of the SNPL arrays and ***d*** is the diameter. Thus, the equal reflectance contour lines are straight lines starting from origin of the plot. This can be explained by the fact that reflection of photons primarily occurs on the top surface of the SNPL arrays and thus the total reflectance largely depends on the top surface area fraction, which is equal to the filling ratio for the uniform diameter SNPL arrays. This effect has been observed experimentally in our previous work [10]. This result indicates that small ***FR*** favors light propagating into an SNPL array. However, in order to

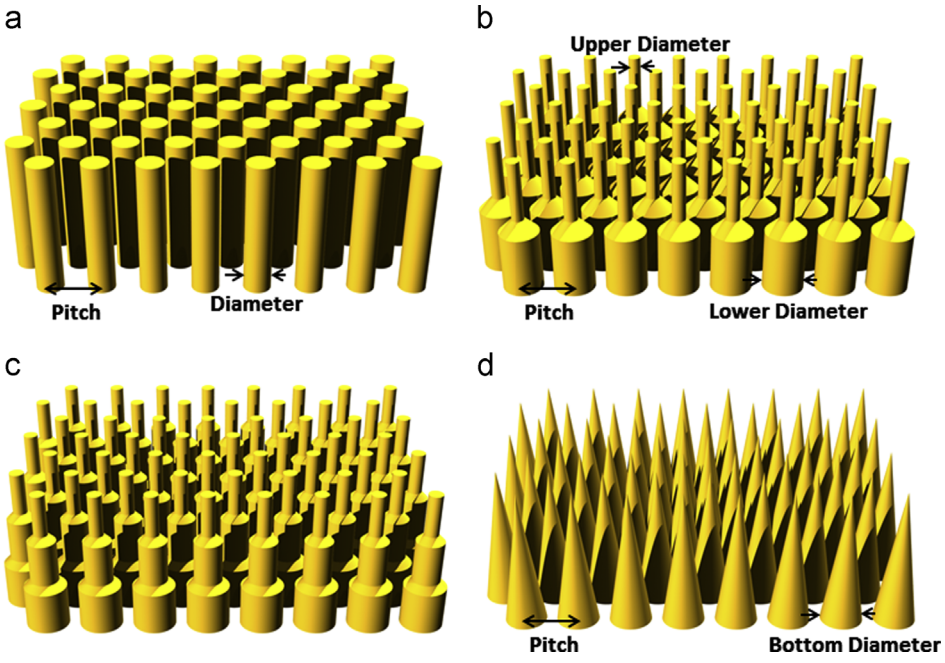

Figure 1 Schematics of hexagonal Ge nanostructure arrays. (a) Single-diameter NPL arrays, (b) Dual-diameter NPL arrays, (c) Multi-diameter NPL arrays and (d) NCN arrays. The parameters mentioned in this work are shown in the figure.

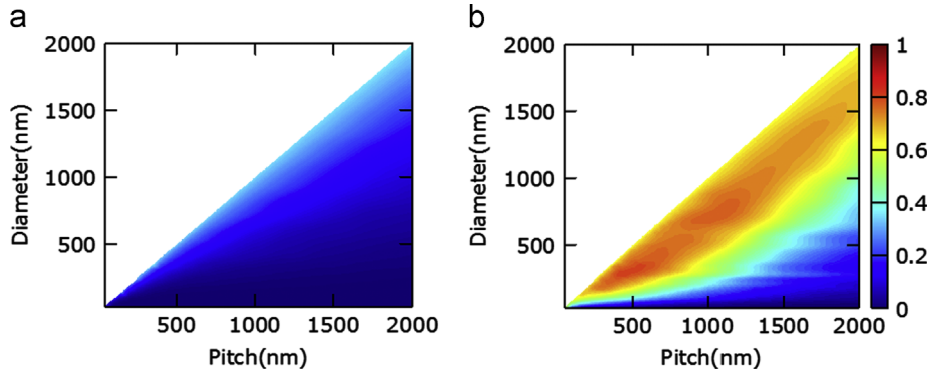

Figure 2 2-D contours of Ge SNPL arrays. (a) Broadband-integrated reflectance and (b) broadband-integrated absorption.

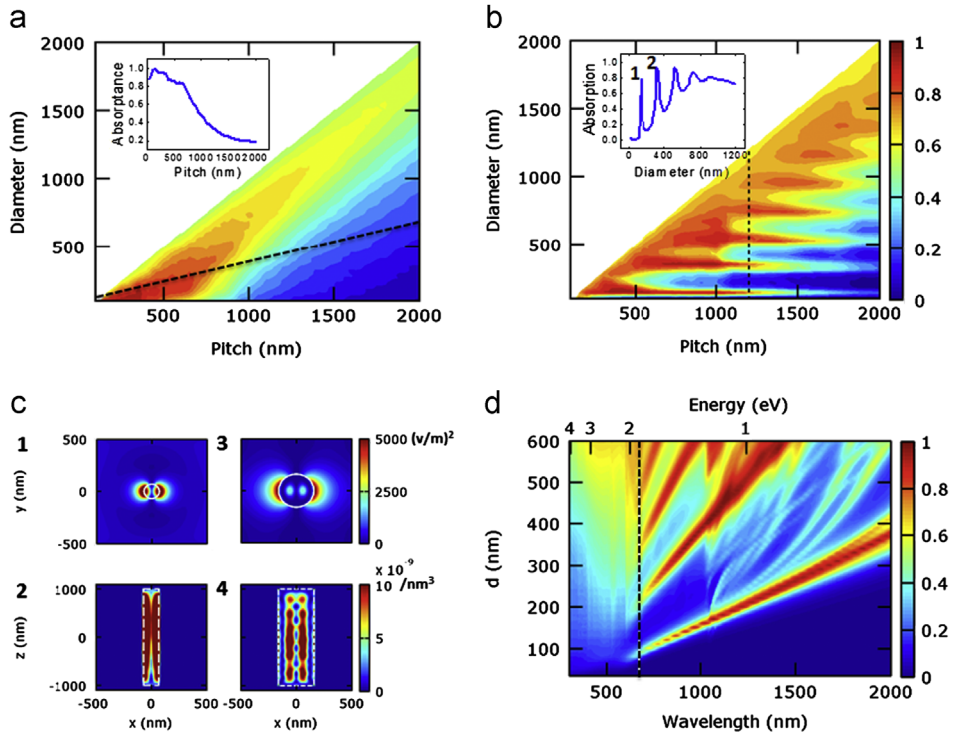

Figure 3 (a) 300 nm wavelength absorption 2-D contour of Ge SNPL arrays. The dashed line corresponds to SNPL arrays with Ge filling ratio of 11%. Inset: the absorption curve on the dashed line. (b) 900 nm wavelength absorption 2-D contour of Ge SNPL arrays. The dashed line corresponds to SNPL arrays with 1200 nm pitch. Inset: 900 nm wavelength absorption curve versus SNPL diameter with 1200 nm pitch. (c)1 (c)3: E field intensity of SNPLs corresponding to peak 1 and 2 in the inset of (b). (c)2 (c)4: Optical absorption cross-section profiles of SNPLs corresponding to peak 1 and 2 in the inset of (b). The diameter of SNPL in (c)1 (c)2 is 140 nm, and the diameter in (c)3 (c)4 is 320 nm. (d) 2-D contour of 1200 nm pitch SNPL arrays absorption with change of wavelength and diameter and diameter. The dashed line corresponds to the peak of photon flux density.

achieve sufficient light absorption, large ***FR*** is desirable. Therefore, after balancing the trade-off between large ***FR*** and small ***FR*** SNPL arrays, the absorption 2-D contour is plotted in Figure 2b, showing that the highest absorption band centers on moderate ***FR***, with the highest solar spectrum integrated absorption ~85%. This result has been confirmed with previous experiments in which optical absorption of fixed-pitch varying-diameter Ge SNPL arrays was explored [10].

It is worth noting that the absorption contour of Figure 2b shows the optimal absorption appears around 500 nm pitch and 300 nm SNPL diameter, even though other pitch-diameter combinations can have the same ***FR***. And it is found that light polarization direction has little impact on the results (Figure S1c), which agrees with the previous work showing symmetry independent light absorption in nanowire arrays [24]. In order to further understand the simulation results, the absorption of SNPLs to individual wavelengths of 300 nm, 600 nm, 900 nm, 1200 nm, 1500 nm and 1800 nm are investigated. For each wavelength, absorption 2-D contours are plotted for comparison. Figure 3a and 3b demonstrate absorption 2-D contours of the short

wavelength of 300 nm and of the long wavelength of 900 nm. And the rest of the wavelengths can be found in Supplementary Figure S2a-d. As shown in Figure 3a, high absorption occurs at pitch less than 300 nm and NPL diameter less than 200 nm, reaching up to 99%. However, the absorption quickly decreases with increasing geometry up to 2000 nm pitch and 700 nm NPL diameter. The inset of Figure 3a shows the geometry dependent absorption along the dashed line with ***FR***=11%. It can be seen that with increase of the pitch, the absorption decreases. In the case that the diameter and pitch of SNPLs are smaller than the input wavelength, the entire structure could be regarded as a uniform light absorbing medium, with an effective absorption coefficient $\alpha_{\text{eff}}(\lambda) = \alpha_{\text{Ge}}(\lambda)FR$, where $\alpha_{Ge}(\lambda)$ is the absorption coefficient of Ge. Since $\alpha_{\text{Ge}}(300\text{ nm}) = 1.56 \times 10^{-1}\text{ nm}^{-1}$ (See Figure S3, absorption coefficient curve), $\alpha_{\text{Eff}}(300\text{ nm}) = 1.7 \times 10^{-2}\text{ nm}^{-1}$, which is still quite significant even with only 11% material filling ratio, leading to high optical absorption capability. This rationale indicates that efficient light absorption can be achieved with small amount of absorbing material fabricated into an array of nanostructures with geometry and interspacing smaller than wavelength, if the material absorption coefficient is sufficient. However, when the SNPL diameter and pitch are much larger than the wavelength, photon reflectance from SNPL top surface and transmittance through the SNPL array structure are in the ray optics regime. With 11% ***FR***, large transmittance loss is expected, leading to low absorption for the large structural geometry shown in Figure 3a. On the other hand, the situation is different when the absorption coefficient is low. For example, $\alpha_{\text{Ge}}(900\text{ nm}) = 2.58 \times 10^{-3}\text{ nm}^{-1}$ (See Figure S3, absorption coefficient curve), which is about two orders of magnitude lower than that at 300 nm. Figure 3b shows a distinctively different 2-D absorption contour as compared to Figure 3a. Particularly, there are horizontal absorption bands showing a 200 nm periodicity on diameter, starting from 150 nm diameter. In other words, the optical absorption capability of SNPLs for 900 nm wavelength is periodically highly sensitive to their diameters, instead of their pitch. The absorption curve as a function of SNPL diameter at 1200 nm pitch is plotted and shown in the inset figure of Figure 3b, showing the absorption oscillation clearly. These high absorption peaks can be attributed to the transverse resonance leaky modes inside SNPLs [25]. However, for short wavelengths, e.g. 300 nm, the high absorption coefficient results in efficient absorption of photon energy quenching the resonance modes.

In order to further uncover the nature of the resonance modes in SNPLs, radial cross-sections of 900 nm wavelength electric field intensity ($|\boldsymbol{E}|^2$) and axial energy loss profiles of individual SNPLs in 1200 nm pitch SNPL arrays with diameter corresponding to first two absorption peaks in Figure 3b inset are plotted and shown in Figure 3c1, c3 and c2, c4, respectively. In general, the optical absorption profile can be calculated as

$$A(\lambda) = \nabla \cdot \left(\frac{1}{2} \text{real}\left(\vec{E}(\lambda) \times \vec{H}(\vec{E}) \right) \right) \tag{2}$$

where $A(\lambda)$ is the absorption per unit volume. It can be clearly seen that the transverse resonance modes in Figure 3c1 and c3 correspond to HE_{11} mode and HE_{12} mode, respectively [20,25]. Therefore, the photon energy can easily couple into these modes leading to significant absorption. Furthermore, a 2-D contour of 1200 nm pitch SNPL arrays with wavelength as the x-axis and diameter as the y-axis is plotted in Figure 3d. It can be clearly seen that when the wavelength is beyond 600 nm, several high absorption bands appear, as shown in the 900 nm

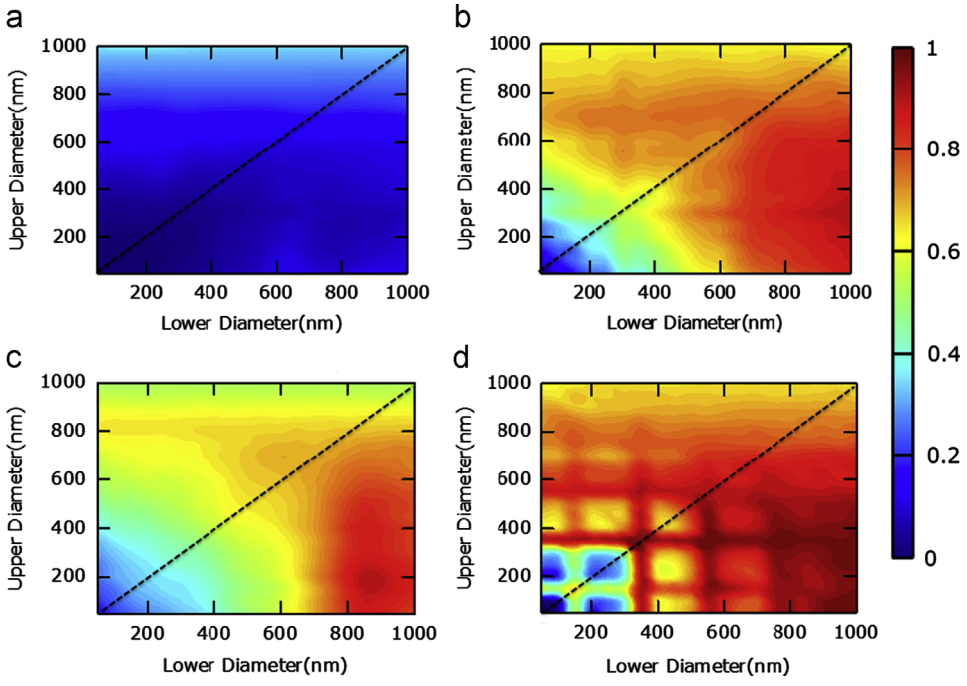

Figure 4 2-D contours of Ge DNPL arrays at 1000 nm pitch. (a) Broadband-integrated reflectance, (b) broadband-integrated absorption, (c) 300 nm wavelength absorption and (d) 900 nm wavelength absorption. The dashed line corresponds to DNPL arrays whose lower diameter is equal to upper diameter, namely SNPL arrays.

wavelength 2-D contour (Figure 3b) and ***E*** field cross-sections (Figure 3c1, c3). These high absorption bands correspond to transverse resonance leaky modes HE_{11}, HE_{12}, HE_{13} etc. The photon energy is more readily to couple into SNPLs as long as the diameter satisfies the transverse resonance condition. On the other hand, larger diameter also leads to increased filling ratio, which can also contribute to high absorption. So the contribution of high order modes like HE_{13} is not as pronounced as the contribution of low order modes such as HE_{11}.

It is worth noting that although Ge is chosen as the model material in this work, the transverse resonance leaky mode theory has also been applied to other materials including Si, amorphous Si and CdTe [2,25,26]. To confirm that our analysis can be extended to other material systems, Si nanopillars have also been investigated in this work. Because the absorption coefficient of Si is much lower than that of Ge at the same wavelength [23], the effect of transverse resonance leaky modes show up for 500 nm wavelength, as opposed to 900 nm wavelength for the case of Ge, as shown in Figure S4b. And the nanopillar diameter difference between each resonance mode is also smaller for this case because of the shorter wavelength. Furthermore, our methodology for investigation can be extended to other photonic materials by considering different refractive indices and absorption coefficients.

Identifying photon energy coupling conditions in uniform diameter NPLs paved the way for understanding optical properties of more complex nanostructures. For example, Figure 4a–d show the optical property investigation of DNPL arrays. The schematic of DNPL arrays is shown in Figure 1b. The total length of a DNPL is set as 2000 nm with each segment ~1000 nm long. A cone structure is used to connect the two segments with a cone angle of 45 degree obtained from previous experiment [10]. The broadband-integrated reflectance 2-D contour of 1000 nm pitch DNPL arrays with variable upper and lower portion diameters (d_{upper}, d_{lower}) is shown in Figure 4a. As discussed previously, the reflectance is mostly determined by the top surface area fraction, therefore it can be seen that the upper NPL diameter dominates the reflectance. However, when the upper diameter is very small, ***e.g.*** 100 nm, the increase of the diameter of the lower part will also marginally increase the total reflectance.

The broadband-integrated absorption of DNPL arrays is shown in Figure 4b. It is obvious that large d_{upper} leads to absorption loss regardless of d_{lower}, as discussed before, and large d_{lower} results in high absorption. Consequently, a broadband absorption of 92% is obtained for a combination of 300 nm d_{upper} and 1000 nm d_{lower}, which is higher than the best absorption of 78% for 1000 nm pitch single diameter NPLs shown in Figure 2b. The conclusion that smaller d_{upper} and larger d_{lower} lead to high absorption agrees well with our previous experimental work, although the pitch and diameters of Ge DNPL here are different from those of the previous one [10]. This result can be explained with the fact that smaller d_{upper} leads to lower effective refractive index and better optical impedance match for the upper structure, and larger d_{lower} comes with higher material filling ratio and better absorption for the lower structure. Interestingly, there are observable absorption pattern lines parallel to x and y-axis in Figure 4b, which intersects with the x- and y-axis at 300 nm and 700 nm. In order to shed light on the origin of these pattern lines, absorption 2-D contours of DNPL arrays with 6 individual wavelengths are obtained. Figure 4c and d show 300 nm and 900 nm wavelength absorption, and Figure S5a–c showing 600 nm, 1200 nm, 1500 nm and 1800 nm wavelength results, corresponding to the wavelengths of Figure 3a, b and Figure S2. Note that for figures of which the wavelengths are equal to or larger than 900 nm, there are both horizontal and vertical absorption pattern lines. It is worth noting that the locations and periodicity of the absorption pattern lines in Figure 4d agree very well with those in Figure 3b for SNPL arrays. This fact indicates the independent existence of transverse resonance modes in each segment of an MNPL leading to the 2-D absorption pattern grid lines. As the broadband input solar photon flux spectrum is not a flat spectrum (Figure S6), the overall absorption is the summation of absorption of each individual wavelength with different weight in the range from 300 nm to 2000 nm. Therefore, the broadband-integrated absorption shows the absorption pattern lines in Figure 4b, which are not as pronounced as these in Figure 4d, Figure S5b–d.

The DNPL structure represents an artificially tapered structure which improves photon coupling efficiency and absorption into three-dimensional nanostructures. On the other hand, it is known that a structure with gradually

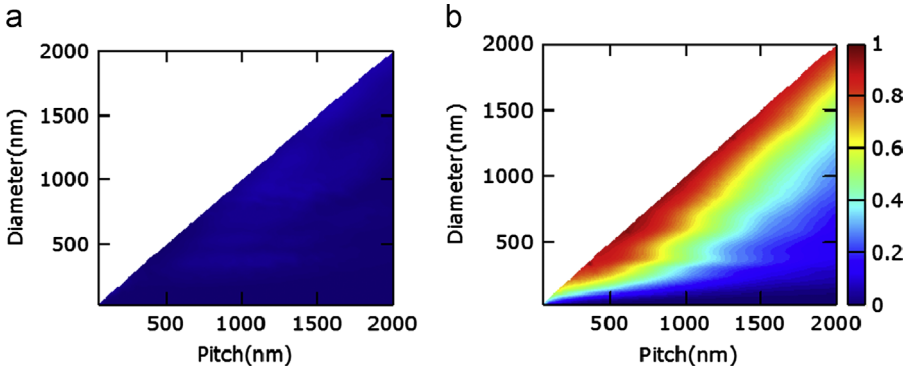

Figure 5 2D contours of Ge NC arrays at 1000 nm pitch. (a) Broadband-integrated reflectance and (b) broadband-integrated absorption.

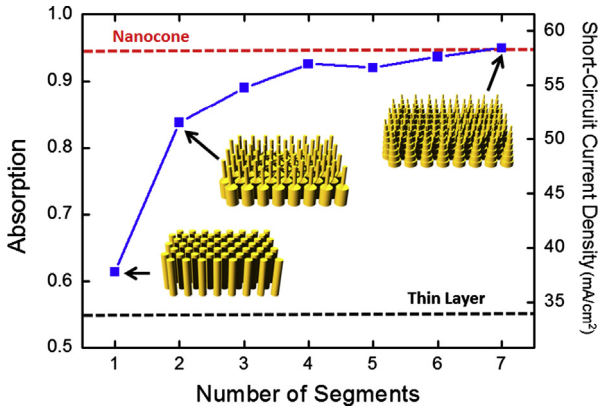

Figure 6 Broadband-integrated absorption of 1000 nm pitch Ge MNPL arrays as a function of segment number. Red dashed line: the broadband-integrated absorption of 1000 nm pitch Ge NC arrays. Black dashed line: the broadband-integrated absorption of 2000 nm Ge thin layer.

increased effective refractive index can serve the same purpose [11,13]. In fact, NCN array structure shown in Figure 1d presents a smooth increase of ***FR*** from the top to the bottom of the structure which will naturally lead to the significant light absorption. In this regard, the broadband-integrated reflectance and absorption of 2000 nm height NCN arrays are plotted and shown in Figure 5a and b, respectively, where the x-axis stands for the pitch, and the y-axis represents the bottom diameter of the NCN. Apparently, the reflectance of NCN arrays is marginal regardless of pitch and bottom diameter, since the cone tip diameter is mathematically zero. And the best absorption for each pitch always appears largest bottom diameter, which echoes with the understanding obtained from DNPLs.

Experimentally, NCN arrays have been largely fabricated with lithography or etching approaches [11,12,15]. These approaches are either costly or hard to guarantee material quality especially at the surface, which is critical for photovoltaic performance. On the other hand, bottom-up growth of DNPL with a template approach [10] demonstrated previously has shown the potency to fabricate MNPL with more smooth structural transition, as shown in Figure 1c. In order to compare the optical absorption capability of MNPLs arrays with NCN arrays and a Ge thin film with the same thickness, 1000 nm pitch MNPLs with ***N*** segments (***N***=1, 2, 3, ...) are constructed and their broadband-integrated absorption and the ideal short current densities (J_{sc}) are calculated and shown in Figure 6. Note that the total height of an MNPL is still fixed at 2000 nm, which is the same with NCN and thin film. Here ***N***=1 represents SNPL. It can be seen that with a diameter equal to pitch, the broadband-integrated absorption of SNPL array is 61.4%, with a corresponding J_{sc} of 37.8 mA/cm^2, which is already higher than that from the Ge thin film. Note that J_{sc} was obtained by integrating AM 1.5 G solar photon flux spectrum (Figure S6) and the absorption spectrum. It suggests the upper limit of the J_{sc} for a solar cell device [27]. It is also observed that the absorption of MNPL arrays increases along with ***N***. Specifically, DNPL shows a significant improvement over SNPL, and the absorption of a 7 segment MNPL array reaches up to 95.1% with a corresponding J_{sc} of 58.4 mA/cm^2, which slightly exceeds that of an NCN array, 95.0% (J_{sc}=58.5 mA/cm^2) for 1000 nm pitch, which is within the simulation error.

Conclusion

In summary, optical properties, particularly absorption capability of arrays of uniform diameter nanopillars, multiple-diameter nanopillars and nanocones are explored here. It is found that the absorption of light in nanopillars can be dominated by either material filling ratio or transverse resonance leaky modes, depending on the wavelength, absorption coefficient and nanopillar diameter. The resonance modes in nanopillars generate periodic absorption pattern lines in the 2-D absorption contour. In addition, it is also found that the MNPL structures can compete with NCN structures with enough segment numbers. These results reveal design guidelines of efficient light harvesting nanostructures for applications such as photovoltaics and photodetection.

Acknowledgment

The authors thank Mr. Qianpeng Zhang for technical assistance. This work was partially supported by General Research Fund (612111) from Hong Kong Research Grants Council, National Research Foundation of Korea funded by the Korean Government (NRF-2010-220-D00060, 2008-0662256), HKUST Special Research Fund Initiative (SRFI11EG17, SRFI11EG17PG-D).

Appendix A. Supporting information

Supplementary data associated with this article can be found in the online version at http://dx.doi.org/10.1016/j.nanoen.2013.03.016.

References

[1] L. Hu, G. Chen, Nano Letters 7 (2007) 3249–3252.
[2] L.Y. Cao, J.S. White, J.S. Park, J.A. Schuller, B.M. Clemens, M. L. Brongersma, Nature Materials 8 (2009) 643–647.
[3] C. Lin, M.L. Povinelli, Optics Express 17 (2009) 19371–19381.
[4] E.C. Garnett, P.D. Yang, Nano Letters 10 (2010) 1082–1087.
[5] J. Kupec, R.L. Stoop, B. Witzigmann, Optics Express 18 (2010) 27589–27605.
[6] K. Seo, M. Wober, P. Steinvurzel, E. Schonbrun, Y. Dan, T. Ellenbogen, K.B. Crozier, Nano Letters 11 (2011) 1851–1856.
[7] P.M. Wu, N. Anttu, H. Xu, L. Samuelson, M.E. Pistol, Nano Letters 12 (2012) 1990–1995.
[8] H. Chang, K. Lai, Y. Dai, H. Wang, C. Lin, J. He, Energy and Environmental Science 4 (2011) 2863–2869.
[9] Z.Y. Fan, H. Razavi, J.W. Do, A. Moriwaki, O. Ergen, Y. L. Chueh, P.W. Leu, J.C. Ho, T. Takahashi, L.A. Reichertz, S. Neale, K. Yu, M. Wu, J.W. Ager, A. Javey, Nature Materials 8 (2009) 648–653.
[10] Z.Y. Fan, R. Kapadia, P.W. Leu, X.B. Zhang, Y.L. Chueh, K. Takei, K. Yu, A. Jamshidi, A.A. Rathore, D.J. Ruebusch, M. Wu, A. Javey, Nano Letters 10 (2010) 3823–3827.

[11] J. Zhu, Z.F. Yu, G.F. Burkhard, C.M. Hsu, S.T. Connor, Y.Q. Xu, Q. Wang, M. McGehee, S.H. Fan, Y. Cui, Nano Letters 9 (2009) 279–282.
[12] S. Jeong, E.C. Garnett, S. Wang, Z. Yu, S. Fan, M. L. Brongersma, M.D. McGehee, Y. Cui, Nano Letters 12 (2012) 2971–2976.
[13] B. Wang, P.W. Leu, Nanotechnology 23 (2012) 194003.
[14] K.X. Wang, Z. Yu, V. Liu, Y. Cui, S. Fan, Nano Letters 12 (2012) 1616–1619.
[15] C.M. Hsu, C. Battaglia, C. Pahud, Z. Ruan, F.J. Haug, S. Fan, C. Ballif, Y. Cui, Advanced Energy Materials 2 (2012) 628–633.
[16] Y.L. Chueh, Z.Y. Fan, K. Takei, H. Ko, R. Kapdia, A. Rathore, N. Miller, K. Yu, M. Wu, E.E. Haller, A. Javey, Nano Letters 10 (2010) 520–523.
[17] S.F. Leung, M. Yu, Q. Lin, K. Kwon, K.L. Ching, L. Gu, K. Yu, Z. Fan, Nano Letters 12 (2012) 3682–3689.
[18] Y. Yao, J. Yao, V.K. Narasimhan, Z. Ruan, C. Xie, S. Fan, Y. Cui, Nature Communications 3 (2012) 664.
[19] R. Yu, K. Ching, Q. Lin, S. Leung, D. Arcrossito, Z. Fan, ACS Nano 5 (2011) 9291–9298.
[20] M.D. Kelzenberg, S.W. Boettcher, J.A. Petykiewicz, D. B. Turner-Evans, M.C. Putnam, E.L. Warren, J.M. Spurgeon, R.M. Briggs, N.S. Lewis, H.A. Atwater, Nature Materials 9 (2010) 239–244.
[21] E.C. Garnett, M.L. Brongersma, Y. Cui, M.D. McGehee, Annual Review of Materials Research 41 (2011) 269–295.
[22] R. Yu, Q. Lin, S.F. Leung, Z. Fan, Nano Energy 1 (2011) 57–72.
[23] J. Nelson (Ed.), Imperial College Press, London, 2003.
[24] J. Li, H.Y. Yu, Y. Li, Nanotechnology 23 (2012) 194010.
[25] B. Wang, P.W. Leu, Optics Letters 37 (2012) 3756–3758.
[26] L. Cao, P. Fan, A.P. Vasudev, J.S. White, Z. Yu, W. Cai, J. A. Schuller, S. Fan, M.L. Brongersma, Nano Letters 10 (2010) 439–445.
[27] Q. Lin, B. Hua, S. Leung, X. Duan, Z. Fan, ACS Nano 7 (2013) 2725–2732.

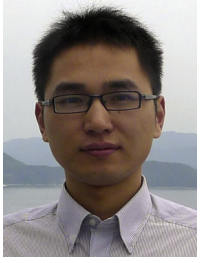

Bo Hua received his B.S. degree in Optical Science and Engineering from Fudan University, Shanghai, China in 2011. He is now a postgraduate student in Department of Electronic and Computer Engineering of Hong Kong University of Science and Technology. His current research interests include simulation and fabrication of nanophotonics based on nanostructures, for application on photovoltaics and other optoelectronics.

Baomin Wang received his Bachelor of Eng. from department of Materials Science and Engineering, Tsinghua University, China, in 2010. And now he is currently pursuing his Ph.D. degree under Dr. Leu in University of Pittsburgh, USA. His research focuses on simulation of nanostructured silicon solar cells and synthesis of silicon nanostructures for solar cells.

Miao Yu received his BSc degree in Physics from Nanjing University, China, in 2010 and received his MPhil degree in Electronic and Computer Engineering from the Hong Kong University of Science and Technology, Hong Kong SAR, in 2012. Currently he is a doctoral candidate in the Mechanical Engineering Department at Columbia University, in the City of New York. His research interests focus on the study of novel nanostructure-based optoelectrical and optomechanical devices.

Dr. Paul W. Leu has been an Assistant Professor in the Department of Industrial Engineering at the University of Pittsburgh since August, 2010. He is the PI of the Laboratory for Advanced Materials at Pittsburgh (LAMP), which focuses on nanomanufacturing and advanced materials design, particularly with respect to solar cells and nanophotonics. He has over 10 publications in journals such as Nature Materials, Nature Nanotechnology, Nano Letters, Physical Review B, and Nanotechnology. His research group's areas of expertise include solar cells, nanomanufacturing, and simulation-based design.

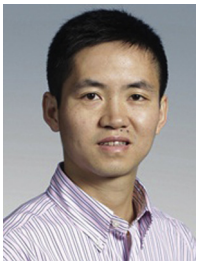

Zhiyong Fan received his B.S. and M.S. degree in physical electronics from Fudan University, Shanghai, China, in 1998 and 2001. He received Ph.D. degree from University of California, Irvine in 2006 in Materials Science. From 2007 to 2010, he worked in University of California, Berkeley as a postdoctoral fellow in department of Electrical Engineering and Computer Sciences, with a joint appointment with Lawrence Berkeley National Laboratory. In May 2010, he joined Hong Kong University of Science and Technology as an assistant professor. His research interets include engineering novel nanostructures with functional materials, for technological applications including energy conversation, electronics and sensors, etc.